

Aspergillus fumigatus strains that evolve resistance to the agrochemical fungicide ipflufenquin in vitro are also resistant to olorofim

Received: 23 February 2023

Accepted: 31 October 2023

Published online: 27 December 2023

Check for updates

Norman van Rhijn¹, Isabelle S. R. Storer¹, Mike Birch², Jason D. Oliver², Michael J. Bottery¹ & Michael J. Bromley¹✉

Widespread use of azole antifungals in agriculture has been linked to resistance in the pathogenic fungus *Aspergillus fumigatus*. We show that exposure of *A. fumigatus* to the agrochemical fungicide, ipflufenquin, in vitro can select for strains that are resistant to olorofim, a first-in-class clinical antifungal with the same mechanism of action. Resistance is caused by non-synonymous mutations within the target of ipflufenquin/olorofim activity, dihydroorotate dehydrogenase (DHODH), and these variants have no overt growth defects.

Invasive aspergillosis (IA), a disease caused primarily by the saprotrophic fungus *Aspergillus fumigatus*, is estimated to cause 500,000 deaths each year (<http://www.gaffi.org/why/burden-of-disease-maps/>). The triazole class of antifungals represents first-line treatments for IA and effectively cures disease in the majority of patients^{1,2}. Correlative data indicate a link between the use of analogous compounds for crop protection and the emergence of triazole resistance in *A. fumigatus*^{3–6}. In some centres, resistance rates now exceed 20% and 9 in 10 patients infected with a resistant strain will succumb to the infection if alternate therapies are not given rapidly^{7–10}. Olorofim, a next-generation antifungal in the orotomide class, is currently in phase III clinical trials for IA and other mould infections and is active against azole-resistant isolates¹¹. Orotomides act by disrupting pyrimidine synthesis via inhibition of dihydroorotate dehydrogenase (DHODH)^{11,12}. As olorofim nears clinical deployment, ipflufenquin, a fungicide that has been shown to be a potent inhibitor of DHODH activity in *Neurospora crassa*¹³, has been approved by the US Environmental Protection Agency for use in agriculture¹⁴ and is under review in other territories¹⁵. There is clear concern that the widespread use of ipflufenquin could drive resistance to the orotomides in *A. fumigatus*.

Our growth inhibition studies confirm that ipflufenquin is active against *A. fumigatus* (minimum inhibitory concentration (MIC)

12.5 mg l⁻¹) at levels that are below the concentration of its use in crop protection (50 mg l⁻¹)¹⁶, and consistent with ipflufenquin acting exclusively by inhibiting DHODH, drug activity can be completely reversed by the addition of exogenous pyrimidines (Fig. 1a and Extended Data Fig. 1). The activity of ipflufenquin was consistent across a collection of 30 natural isolates (Extended Data Fig. 2a) (12.5 mg l⁻¹) and similarly, all isolates had the same MIC to olorofim of 0.075 mg l⁻¹ (Extended Data Fig. 2b,c). By comparing the area under the curve (AUC) calculated from the drug dose-response curves, we were able to detect a correlation in the ability of strains to grow in sub-MICs of olorofim and ipflufenquin (Extended Data Fig. 2d; $R^2 = 0.7731$, $P = 7.8 \times 10^{-12}$).

Using an Alphafold2 generated model of the *A. fumigatus* (*Af*) DHODH (Extended Data Fig. 3), we predict that both ipflufenquin and olorofim bind effectively within the active site of the enzyme (binding energies: orotate -7.0 kcal mol⁻¹, flavin mononucleotide (FMN) -10.8 kcal mol⁻¹, olorofim -8.2 kcal mol⁻¹, ipflufenquin -9.2 kcal mol⁻¹) (Fig. 1b). The most energy-favourable poses indicate that the larger olorofim molecule but not ipflufenquin extends from the active site across the entry channel (Extended Data Fig. 4). Consistent with the model, ipflufenquin directly inhibits the enzymatic activity of *Af*DHODH, although the half maximal inhibitory concentration (IC₅₀) is more than 15 times higher than that previously observed for olorofim (IC₅₀: 0.77 μM ipflufenquin vs 0.044 μM olorofim; Fig. 1c)^{11,17}.

¹Manchester Fungal Infection Group, Division of Evolution, Infection, and Genomics, Faculty of Biology, Medicine and Health, The University of Manchester, Manchester, UK. ²F2G Ltd, Manchester, UK. ✉e-mail: Mike.Bromley@manchester.ac.uk

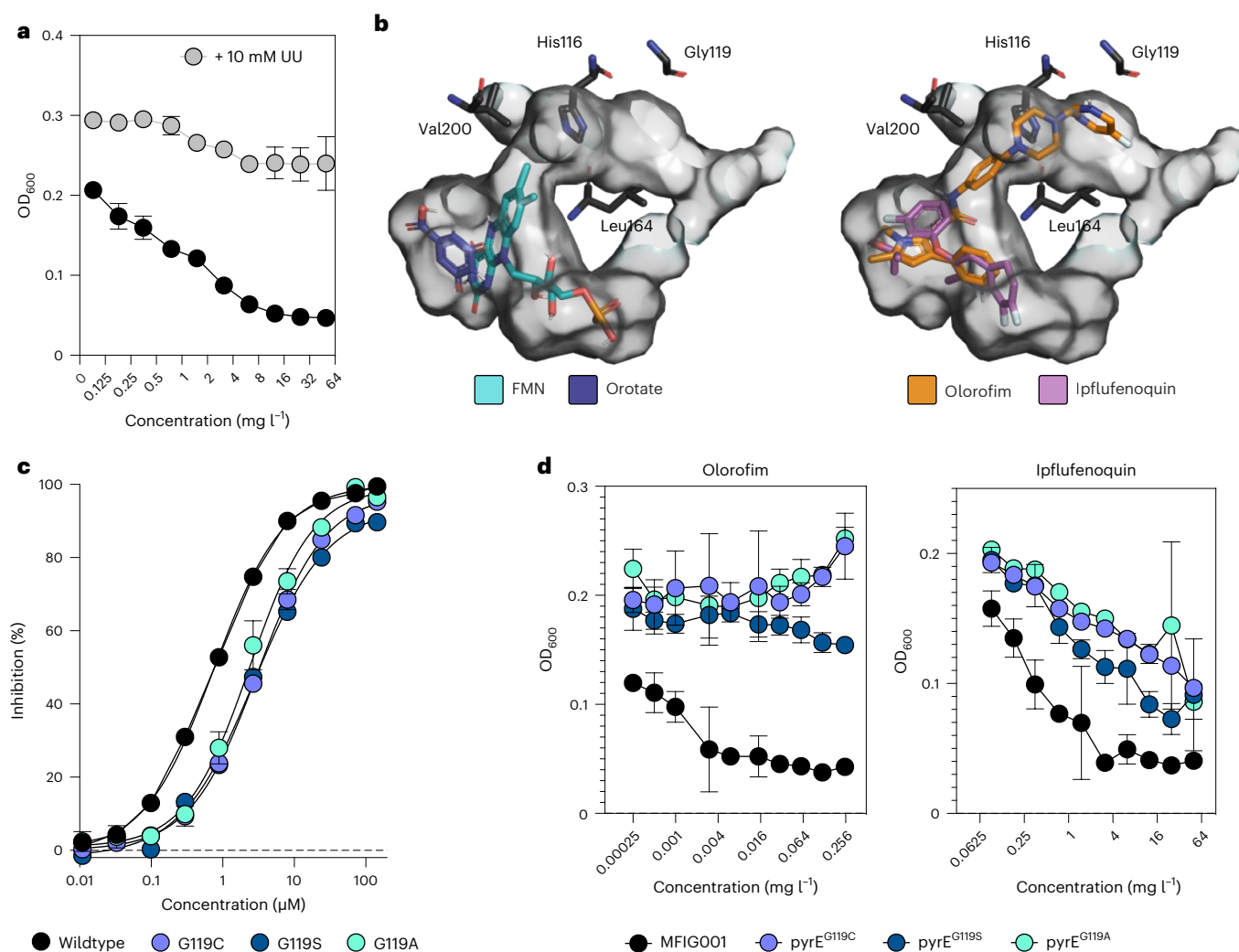


Fig. 1 | Ipflufenzoquin acts against DHODH. **a**, MIC determination of ipflufenzoquin (0.175–50 mg l⁻¹) against *A. fumigatus* MFIG001 in RPMI-1640 (black) using the EUCAST methodology and with addition of 10 mM uridine and uracil (grey). OD₆₀₀ was measured after 48 h. Three biological replicates were assessed. Data are presented as mean ± s.e.m. **b**, Molecular docking of FMN and orotate (left in cyan and blue, respectively) and Olorofim and ipflufenzoquin (right, orange and purple, respectively) to an AlphaFold2 model of *A. fumigatus*

DHODH. The pocket of the active site is shown in grey. **c**, Protein inhibition assay of ipflufenzoquin towards wildtype and G119 variants of DHODH. At least five biological replicates were assessed. Data are presented as mean ± s.e.m. (n = 5). **d**, MIC determination of G119 variants (G119C, G119S and G119A) against ipflufenzoquin (right) and Olorofim (left) according to EUCAST methodology. OD₆₀₀ was measured after 48 h. Three biological replicates were assessed. Data are presented as mean ± s.e.m.

Non-synonymous small nucleotide polymorphisms (SNPs) at bases 355 (G to A/T) and 356 (G to T) of the *pyrE* gene equivalent to amino acid position G119 (G119C, G119S or G119A) at the entrance to the active site (Fig. 1b) of (*Af*)DHODH are sufficient to provide high-level resistance (>8 mg l⁻¹) to Olorofim¹⁷. To assess whether these mutations result in cross-resistance to ipflufenzoquin, we generated isolates containing the variants (Extended Data Fig. 5)¹⁸. All variants were resistant to the highest concentration of Olorofim tested in our assay (>0.3 mg l⁻¹) (Fig. 1d and Extended Data Fig. 1). Although our predictions indicate that ipflufenzoquin does not interact directly with G119, these mutants were cross-resistant to ipflufenzoquin (>50 mg l⁻¹) (Fig. 1d and Extended Data Fig. 1), suggesting that G119 mutations either result in a conformational change of the active site that affects the ability of ipflufenzoquin to bind or restricts access to the active site via the entry channel. Mirroring this, *Af*DHODH protein variants G119C, G119S and G119A had marked increases in IC₅₀s to Olorofim (IC₅₀ >100 μM¹⁷) and ipflufenzoquin (IC₅₀ 3.3 μM, 3.3 μM and 2.5 μM, respectively; Fig. 1c).

Using a hypermutator strain of *A. fumigatus* (Δ *pmsA* (*AFUB_029050*); orthologue of *E. coli* mutL), we identified 9 ipflufenzoquin-resistant isolates (Extended Data Fig. 6a). Sequencing

of the *pyrE* gene revealed SNPs at three loci: H116R (n = 3 isolates), L164P (n = 3) and V200E (n = 3) (Extended Data Fig. 7). These mutants were resistant to ipflufenzoquin (>50 mg l⁻¹) and Olorofim at levels exceeding the published MIC₉₀ for *A. fumigatus* (>0.3 mg l⁻¹) (Extended Data Figs. 1 and 6b)¹⁹.

To confirm that the polymorphisms identified in our hypermutator isolate were directly linked to the ipflufenzoquin-resistance phenotype, we reconstructed the SNPs in an isotype background (*A. fumigatus* MFIG001)¹⁷. Strains harbouring the three variants (n = 2 independent isolates for each) displayed high-level resistance to ipflufenzoquin (MIC > 50 mg l⁻¹) (Fig. 2a and Extended Data Fig. 1), were cross-resistant to Olorofim at the highest concentrations tested (MIC > 0.3 mg l⁻¹) (Fig. 2a and Extended Data Fig. 1) and exceeded the MIC observed for any of the natural isolates tested. Evaluation of the AUC from the drug dose-response curves revealed significant decreases in the susceptibility of the mutants to the inhibitors at sub-MIC levels when compared with the isotype strain (Extended Data Fig. 8) and the natural isolate collection. The mutants isolated from Olorofim (G119A and G119C) were less susceptible to Olorofim than those selected on ipflufenzoquin (H116R, L164P and V200E) and vice versa (Extended Data Fig. 8 and

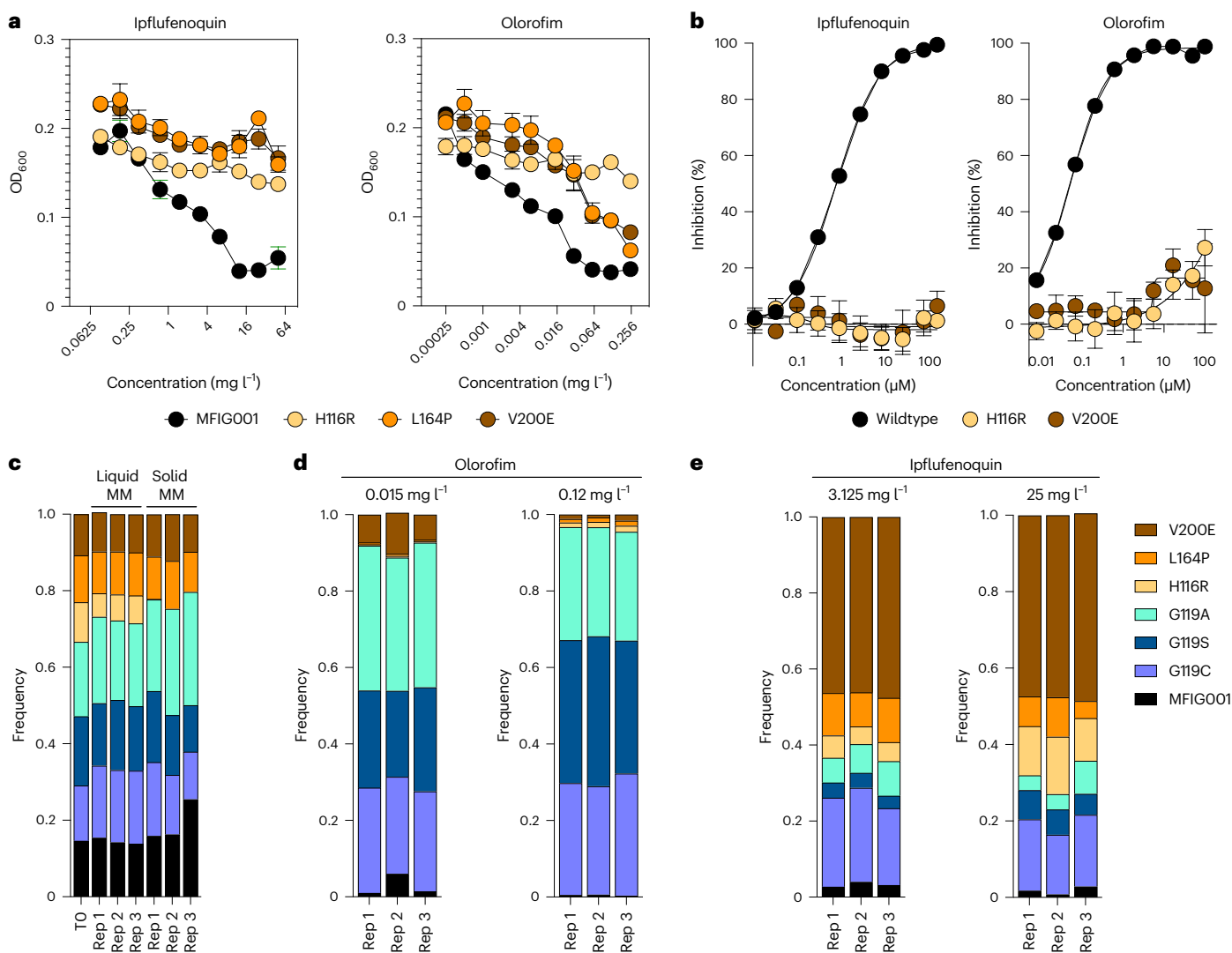


Fig. 2 | Ipflufenquin can select for orlofim-resistant *A. fumigatus*. **a**, MIC determination of H116R, L164P and V200E variant mutants against ipflufenquin and orlofim according to EUCAST methodology. OD₆₀₀ was measured after 48 h. Three biological replicates were assessed. Data are presented as mean ± s.e.m. **b**, Protein inhibition assay of ipflufenquin towards wildtype, V200E and H116R variants of DHODH. At least five biological replicates were assessed. Data are presented as mean ± s.e.m. ($n = 5$). **c**, Frequency of mutants after mixed-inoculum experiments to determine basal fitness of each mutant on solid and liquid MM

medium. Three biological replicates were assessed and individual data from replicates are shown. **d**, Frequency of mutants after low (0.015 mg l⁻¹) and high (0.12 mg l⁻¹) orlofim challenge in a mixed-inoculum competition assay. Three biological replicates were assessed and individual data from replicates are shown. **e**, Frequency of mutants after low (3.125 mg l⁻¹) and high (25 mg l⁻¹) ipflufenquin challenge in a mixed-inoculum competition assay. Three biological replicates were assessed and individual data from replicates are shown.

Supplementary Table 1). Enzyme activity of *Af*DHODH proteins with the variants H116R and V200E was only modestly inhibited by either ipflufenquin or orlofim even at the highest concentration tested (IC₅₀ > 100 μM; Fig. 2b).

Mutations that confer resistance are often associated with a cost to fitness or reduced sporulation that impact the ability of strains to become widely distributed. Radial growth assays of the resistant mutants showed that only strains with the H116R and L164P variants had reduced growth rates (Extended Data Fig. 9a,b; $P < 0.0001$ for both variants), while only the mutant harbouring the H116R variant had a significant sporulation defect ($P < 0.001$) (Extended Data Fig. 9c). To model the fitness of the resistant variants in a competitive context, we created a mixed inoculum with isolates that harbour the 6 DHODH variants and the parental MFIG001 isolate, allowed the strains to compete in co-culture, and using a process analogous to Bar-seq²⁰, we evaluated the abundance of each strain at the beginning and end of the experiment. In the absence of drug pressure, the H116R variant

showed reduced competitive fitness in both liquid and solid *Aspergillus* minimal media (AMM), replicating the outcome of the radial growth and sporulation experiments (Fig. 2c); however, no competitive disadvantage was observed for the other strains. Upon exposure to sub-inhibitory concentrations of orlofim (0.015 mg l⁻¹) in solid media, the G119C, G119A and G119S variants increased in frequency while the H116R, L164P and V200E variants were detected at a lower frequency, suggesting that the latter variants are less fit than the G119 variants under orlofim selection (Fig. 2d). At higher concentrations of orlofim (0.12 mg l⁻¹), the selective advantage of the G119 variants was further exacerbated (Fig. 2d; $P < 0.001$ by one-way analysis of variance (ANOVA)); however, the L164P, H116R and V200E had improved fitness when compared directly with the isotype strain ($P = 0.038$, $P = 0.0314$, $P = 0.0312$ by one-way ANOVA, respectively). Conversely, the isolate containing the V200E variant dominated populations that were exposed to ipflufenquin (Fig. 2e). Notably, even under high ipflufenquin stress, the G119C mutant had enhanced fitness when

compared with the isotype control ($P = 0.01$). The H116R-containing strain also had enhanced fitness in ipflufenquin in a dose-responsive manner despite its high inherent fitness cost (Fig. 2e). The ability of the G119 mutants to dominate the population under olorofim exposure and the V200E isolate under ipflufenquin exposure was maintained in RPMI-1640 liquid culture (Extended Data Fig. 10). The L164P mutant, which exhibited a growth defect in isolated culture, did not appear to have a fitness defect when in competition, suggesting that nutrient exchange (cross-feeding) between strains may mitigate the growth impact caused by the mutation.

Our experiments are unable to replicate the complexities and vast variation that natural environmental settings pose; however, the lack of fitness defects in the laboratory settings tested here indicates that there are no obvious barriers to resistant strains surviving and becoming dominant in the environment. Furthermore, we cannot exclude the possibility that strains carrying variants that impact fitness, such as H116R, could accumulate compensatory mutations elsewhere in the genome that would ameliorate the initial fitness defect caused by the mutation.

It has been suggested that the widespread use of agricultural demethylase inhibitors is driving cross-resistance to the triazoles in *A. fumigatus*^{3,5}. Our results show that the use of ipflufenquin can similarly select for cross-resistance to the first-in-class orotomide, olorofim. The consequences of this are unclear; however, if resistance to the next-generation clinical antifungals is again driven by the use of agrochemicals, we will be limiting our future ability to treat *A. fumigatus* and potentially other filamentous fungal infections¹¹. Despite the clear need for new fungicides to enhance food security²¹, we would advise that, before approval of ipflufenquin for widespread commercial use, field trials are performed to (1) assess the likelihood that olorofim-resistant *A. fumigatus* will emerge via exposure to ipflufenquin and (2) identify high-risk practices that have the potential to provide hotspots for resistance emergence and subsequent spread²².

Methods

Strains, culture conditions and antifungals

A. fumigatus MFIG001 was used as the parental isolate to generate all mutants by selection-free clustered regularly interspaced short palindromic repeats (CRISPR)-Cas9-mediated transformation^{18,23}. *A. fumigatus* wildtype isolates ($n = 30$) representing the full genetic diversity within the population were provided by Matthew Fisher⁵. Unless otherwise stated, *A. fumigatus* strains used in this study were cultured on Sabouraud dextrose agar (Oxoid) for 3 d at 37 °C and collected in phosphate buffered saline (PBS) + 0.01% Tween-20. Olorofim was synthesized by Concept Life Sciences. Ipflufenquin powder (>98% analytical grade) was obtained from CRM LabStandard. The fluctuation assay was performed by inoculating 1×10^6 spores per well from 7 independent *A. fumigatus* $\Delta pmsA$ cultures into 8 wells containing *Aspergillus* MM medium²⁴ + 5 mg l⁻¹ ipflufenquin. After 4 d of incubation at 37 °C, spores from wells containing growth were transferred to Sabouraud agar and grown at 37 °C for 3 d (Fig. 2a). Spores were collected in PBS + 0.01% Tween-20 and stored at -80 °C.

Susceptibility testing

MIC determination for all drugs was carried out according to methods outlined by EUCAST ($n = 3$)²⁵. Spores were inoculated per well of a CytoOne 96-well plate (StarLab) containing RPMI-1640 medium, 2.0% glucose and 165 mM MOPS buffer (pH 7.0) with a range of drug (olorofim 0.00025–0.3 mg l⁻¹, ipflufenquin 0.17–50 mg l⁻¹). Plates were incubated at 37 °C for 48 h and optical density (OD) measurements were taken at 600 nm.

Protein purification and activity assay

The cloning of *A. fumigatus* DHODH_(89–531) complementary DNA into protein expression vector pET44 (ref. 11) and the subsequent mutation of the Gly119 site to cysteine (G2S), valine (G2V), alanine (G2A) and

serine (G2S) have been described previously¹⁷. His116 was mutated to arginine (H2R) and Val200 was mutated to glutamic acid (V2E) using the Phusion Site-Directed Mutagenesis kit (ThermoFisher) with pET44 *A. fumigatus* DHODH_(89–531) as the template. Primers were CCGAAGAG-CGCGTCATATTGGTGT and CGTCGGGATAAAGCGTCCGG for H2R and CCGGACCTCGTGAGTTCGACTGCC and GATTGCCCTCTGTGGCAGG for V2E mutagenesis. Expression of the various proteins in *E. coli* BL21 (DE3) cells (Merck) and purification by immobilized metal-affinity chromatography were followed by DHODH assay according to previously described protocol¹¹. Mutagenesis of Lys164 to proline was also achieved, but the *E. coli* expressed protein was insoluble. DHODH assays were set up in the presence and absence of ipflufenquin at concentrations between 0.01 and 144 μM. Assays were carried out in 50 mM Tris HCl (pH 8), 150 mM KCl, 10% (w/v) glycerol and 0.1% (w/v) Triton X-100 in the presence of 1 mM L-dihydroorotic acid, 0.05 mM coenzyme Q2 and 0.1 mM 2,6-dichloroindophenol as a redox indicator. Activity was determined by the decrease in absorbance at 600 nm and reaction velocities used to construct IC₅₀ curves in XLfit 5.5.0 (IDBS).

In silico protein prediction and docking

The structure of DHODH was determined using AlphaFold2 (ref. 26); for subsequent analysis, the highest-scoring model was used (pLDDT: 96.1, pTMscore: 0.9375). VSpice²⁷, a semi-automated pipeline that utilizes MGLTools (1.5.6) and AutoDock Vina (1.1.2), was used for targeted docking with the ligands and antifungals at the quinone binding pocket. The grid centre for the generated protein data bank (PDB) file was $x = -2.582$, $y = -5.147$ and $z = -4.552$. The grid spacing was set to the default of 0.375 Å and the box size was $30 \times 30 \times 30$ Å³ to encompass the whole tunnel leading to the active site²⁸. The 9 most-energy-favourable outputs (that is, with the lowest predicted binding free energy (ΔG)) were visualized in PyMOL 2.5 (Extended Data Fig. 4).

Selection-free CRISPR-Cas9-mediated transformation

For transforming MFIG001, CRISPR RNAs (crRNAs) were designed to target the intron of the *pyrE* gene in A1163. The closest PAM site with scores >0.5, as calculated by EuPaGDT, was used, and 20-bp crRNAs were ordered from IDT (crRNA: GTATACCCGAAGACTGCAT). CRISPR transformation was performed as previously described¹⁸. Briefly, *A. fumigatus* was grown overnight at 37 °C in Sabouraud agar, followed by protoplasting using Vinotaste. Protoplasts were washed twice in 0.6 M KCl, followed by resuspension in 0.6 KCl + 200 mM CaCl₂. Guide RNA was formed by annealing crRNA to trans-activating CRISPR RNA (IDT) and ribonucleoproteins (RNPs) were formed by incubating at room temperature for 5 min with purified SpCas9 (IDT). The substrate for repair template synthesis (double-stranded (ds)DNA) was obtained by PCR amplification of *pyrE* from ipflufenquin-resistant $\Delta pmsA$ isolates (primers: ACGCAAGAGGAACAGAGGAA and GGATGTTTCTGGGAG-GTTT). Single-stranded (ss)DNA repair template was obtained via lambda exonuclease degradation of the 5' phosphorylated DNA strand. Any remaining dsDNA was degraded by Exonuclease I. This mixture was column purified (Geneflow). Single-strand repair template, RNPs and protoplasts were mixed with PEG-CaCl₂ and incubated for 50 min on ice. PEG-CaCl₂ (600 μl) was added, followed by incubation at room temperature for 20 min. Protoplasts were spread onto YPS medium, left at room temperature for 1 d, followed by incubation at 37 °C for 3 d. Transformants were purified and duplicate spot tests onto Sabouraud agar with and without antifungal (ipflufenquin or olorofim) were performed to confirm resistance. Transformants were validated by Sanger sequencing the entire *pyrE* region introduced in the transformant isolates using primer AGTAAAGGAGGCCACCAAGAAAGCTGG (Genewiz).

Phenotypic analysis

Spores (10^3) of strains were spot inoculated onto the centre of solid Sabouraud agar plates. Plates were incubated for 48 h at 37 °C and measurements or images were taken. Sporulation assays were performed

by culturing all isolates on Sabouraud dextrose agar for 4 d. Spore solutions were normalized to 5×10^6 spores per ml, 50 μ l was spread onto culture flasks containing AMM²⁴ and incubated for 3 d at 37 °C. Spores were collected into 10 ml PBS + 0.01% Tween-20 through filtration over Miracloth and counted on a haemocytometer.

Competition assays

Conidia were harvested from 3-day-old Sabouraud dextrose agar cultures using PBS + 0.01% Tween-20 (PBS-T) and collected by filtration through Miracloth (Millipore, 475855). Spores were quantified using a haemocytometer, normalized to 5×10^6 spores per ml and pooled into one tube. For the solid AMM medium in vitro competitive fitness, the spore pool was diluted to 5×10^4 spores per ml and 100 μ l was plated onto solid AMM. Plates were incubated at 37 °C for 3 d. For the liquid RPMI-1640 in vitro competitive fitness assay, 1 ml of the pool of DHODH mutants and MFIG001 was added to each flask containing 10 ml RPMI-1640. All experiments were performed in triplicate and incubated in a shaking incubator at 120 r.p.m. for 24 h at 37 °C. For low and high olorofim concentrations, 0.015 mg l⁻¹ and 0.12 mg l⁻¹ were used, respectively, whereas for ipflufenquin, 3.125 mg l⁻¹ (low) and 25 mg l⁻¹ (high) were used.

After incubation, plates and flasks were removed from the incubator and the spores (from each plate) or biomass (from each flask) were respectively collected using Miracloth and a Büchner funnel under vacuum. Liquid nitrogen was used to snap freeze the biomass, which was ground into a powder using a sterile mortar and pestle. From each baffled flask, 0.1 g was collected for DNA extraction. Total fungal DNA was extracted using a standardized CTAB DNA extraction²⁹. Enrichment PCR (primers: TATGCTGTGGTTCCTCTTG and GTTGATCATGGCTTCTGA) was performed using PhusionFlash polymerase and primers amplifying the *pyrE* gene for 1 cycle at 98 °C for 30 s, followed by 30 cycles at 98 °C for 10 s, 65 °C for 30 s, 72 °C for 30 s and a final extension step at 72 °C for 10 min. Enriched products were cleaned using AMPure beads and indexed with the Nextera XT kit (NEB) following manufacturer protocol. Sequencing was performed on an Illumina iSeq system following manufacturer protocol. Raw reads were quality controlled using FastQC and trimmed using Trimmomatic v.0.38.0. Trimmed reads were aligned to the A1163 *pyrE* gene using HISAT2 v.2.2.21; only reads over 145 bp were included to cover all SNPs. BAM files were exported to IGV v.2.8.13, from which the abundance of each SNP was assessed by counting the number of reads containing SNP-associated bases at individual genomic locations. A minimum of 8,000 reads per sample was analysed (range 8,281–135,184). The relative abundance of each strain was assessed using IGV by dividing the total reads containing an SNP by the total aligned reads for each sample.

Statistical analysis

Statistical analysis was performed using Graphpad Prism 9 software. Differences among groups were analysed using a one-way ANOVA with Dunnett's test. IC₅₀ curves were analysed using XLfit 5.5.0 (IDBS).

Reporting summary

Further information on research design is available in the Nature Portfolio Reporting Summary linked to this article.

Data availability

Source Data are provided with this paper. Raw sequencing reads are available at SRA: [PRJNA961782](https://www.ncbi.nlm.nih.gov/sra/PRJNA961782). Human DHODH PDB file was obtained from 2PRH_1 (<https://www.rcsb.org/structure/2prh>). Correspondence and requests for materials should be addressed to M.J. Bromley.

References

- Herbrecht, R. et al. Voriconazole versus amphotericin B for primary therapy of invasive aspergillosis. *N. Engl. J. Med.* **347**, 408–415 (2002).
- Patterson, T. F. et al. Executive summary: practice guidelines for the diagnosis and management of aspergillosis: 2016 update by the Infectious Diseases Society of America. *Clin. Infect. Dis.* **63**, 433–442 (2016).
- Snelders, E. et al. Triazole fungicides can induce cross-resistance to medical triazoles in *Aspergillus fumigatus*. *PLoS ONE* **7**, e31801 (2012).
- Fraaije, B. et al. The multi-fungicide resistance status of *Aspergillus fumigatus* populations in arable soils and the wider European environment. *Front. Microbiol.* **11**, 599233 (2020).
- Rhodes, J. et al. Population genomics confirms acquisition of drug-resistant *Aspergillus fumigatus* infection by humans from the environment. *Nat. Microbiol.* **7**, 663–674 (2022).
- Bromley, M. J. et al. Occurrence of azole-resistant species of *Aspergillus* in the UK environment. *J. Glob. Antimicrob. Resist.* **2**, 276–279 (2014).
- Bueid, A. et al. Azole antifungal resistance in *Aspergillus fumigatus*: 2008 and 2009. *J. Antimicrob. Chemother.* **65**, 2116–2118 (2010).
- Buil, J. B. et al. Trends in azole resistance in *Aspergillus fumigatus*, the Netherlands, 1994–2016. *Emerg. Infect. Dis.* **25**, 176–178 (2019).
- Steinmann, J. et al. Emergence of azole-resistant invasive aspergillosis in HSCT recipients in Germany. *J. Antimicrob. Chemother.* **70**, 1522–1526 (2015).
- van Paassen, J. et al. Emerging aspergillosis by azole-resistant *Aspergillus fumigatus* at an intensive care unit in the Netherlands, 2010 to 2013. *Eur. Surveill.* <https://doi.org/10.2807/1560-7917.es.2016.21.30.30300> (2016).
- Oliver, J. D. et al. F901318 represents a novel class of antifungal drug that inhibits dihydroorotate dehydrogenase. *Proc. Natl Acad. Sci. USA* **113**, 12809–12814 (2016).
- van Rhijn, N. et al. Antagonism of the azoles to olorofim and cross-resistance are governed by linked transcriptional networks in *Aspergillus fumigatus*. *mBio* **13**, e0221522 (2022).
- Fujii, S. Features of the new fungicide quinoprol (ipflufenquine). *Plant Prot.* **77**, 164–166 (2023).
- Bo-geun, B. & Oh-jin, K. Introduction of the new fungicide, KINOPROL®. *Proceedings of the Korean Society of Pesticide Science Conference* 125–131 (2022).
- Umetsu, N. & Shirai, Y. Development of novel pesticides in the 21st century. *J. Pestic. Sci.* **45**, 54–74 (2020).
- Hirayama, K. Curative effects of fungicides against *Venturia inaequalis* causing apple scab. *J. Gen. Plant Pathol.* **88**, 264–269 (2022).
- Buil, J. B. et al. Resistance profiling of *Aspergillus fumigatus* to olorofim indicates absence of intrinsic resistance and unveils the molecular mechanisms of acquired olorofim resistance. *Emerg. Microbes Infect.* **11**, 703–714 (2022).
- van Rhijn, N. et al. Development of a marker-free mutagenesis system using CRISPR-Cas9 in the pathogenic mould *Aspergillus fumigatus*. *Fungal Genet. Biol.* **145**, 103479 (2020).
- Astvad, K. M. T. et al. Olorofim susceptibility testing of 1,423 Danish mold isolates obtained in 2018–2019 confirms uniform and broad-spectrum activity. *Antimicrob. Agents Chemother.* **65**, e01527–20 (2020).
- Macdonald, D. et al. Inducible cell fusion permits use of competitive fitness profiling in the human pathogenic fungus *Aspergillus fumigatus*. *Antimicrob. Agents Chemother.* **63**, e01615-18 (2019).
- Stukenbrock, E. & Gurr, S. Address the growing urgency of fungal disease in crops. *Nature* **617**, 31–34 (2023).
- Schoustra, S. E. et al. Environmental hotspots for azole resistance selection of *Aspergillus fumigatus*, the Netherlands. *Emerg. Infect. Dis.* **25**, 1347–1353 (2019).

23. Bertuzzi, M. et al. On the lineage of *Aspergillus fumigatus* isolates in common laboratory use. *Med. Mycol.* **59**, 7–13 (2021).
24. Pontecorvo, G. et al. The genetics of *Aspergillus nidulans*. *Adv. Genet.* **5**, 141–238 (1953).
25. Arendrup, M. C. et al. EUCAST technical note on *Aspergillus* and amphotericin B, itraconazole, and posaconazole. *Clin. Microbiol. Infect.* **18**, E248–50 (2012).
26. Jumper, J. et al. Highly accurate protein structure prediction with AlphaFold. *Nature* **596**, 583–589 (2021).
27. Alvarez-Carretero, S. et al. VSpire, an integrated resource for virtual screening and hit selection: applications to protein tyrosine phosphatase inhibition. *Molecules* **23**, 353 (2018).
28. Trott, O. & Olson, A. J. AutoDock Vina: improving the speed and accuracy of docking with a new scoring function, efficient optimization, and multithreading. *J. Comput. Chem.* **31**, 455–461 (2010).
29. Fraczek, M. G. et al. The cdr1B efflux transporter is associated with non-cyp51a-mediated itraconazole resistance in *Aspergillus fumigatus*. *J. Antimicrob. Chemother.* **68**, 1486–1496 (2013).

Acknowledgements

We thank T. Furukawa for help with translating Japanese articles. N.v.R. was supported by Wellcome Trust (grant: 226408/Z/22/Z), I.S.R.S. was supported by an MRC DTP Studentship, M. J. Bottery was supported by Wellcome Trust (grant: 221653/Z/20/Z), M. J. Bromley was supported by Wellcome Trust (grant: 219551/Z/19/Z and 208396/Z/17/Z).

Author contributions

N.v.R. designed, performed and analysed experiments, wrote and reviewed the manuscript. I.S.R.S. designed, performed and analysed experiments and wrote the manuscript. M.B. and J.D.O. designed, performed and analysed experiments. M. J. Bottery performed and analysed experiments and wrote the manuscript. M. J. Bromley designed and analysed experiments, wrote and reviewed the manuscript and managed grants.

Competing interests

M. J. Bromley is a former employee of F2G Ltd (until 2007), the company that developed the antifungal olorofim. He has received historic funding for PhD studentships from F2G Ltd but has no current financial interest in F2G Ltd. M.B. and J.D.O. are employed by F2G Ltd.

Experiments carried out at the University of Manchester were done independently and without input or incumbrance from F2G Ltd. F2G Ltd contribution was solely in relation to the IC₅₀ analysis of AfDHODH variants. All remaining authors declare no competing interests.

Additional information

Extended data is available for this paper at <https://doi.org/10.1038/s41564-023-01542-4>.

Supplementary information The online version contains supplementary material available at <https://doi.org/10.1038/s41564-023-01542-4>.

Correspondence and requests for materials should be addressed to Michael J. Bromley.

Peer review information *Nature Microbiology* thanks Kentaro Tomii, Jacques Meis, Tom Chiller and the other, anonymous, reviewer(s) for their contribution to the peer review of this work.

Reprints and permissions information is available at www.nature.com/reprints.

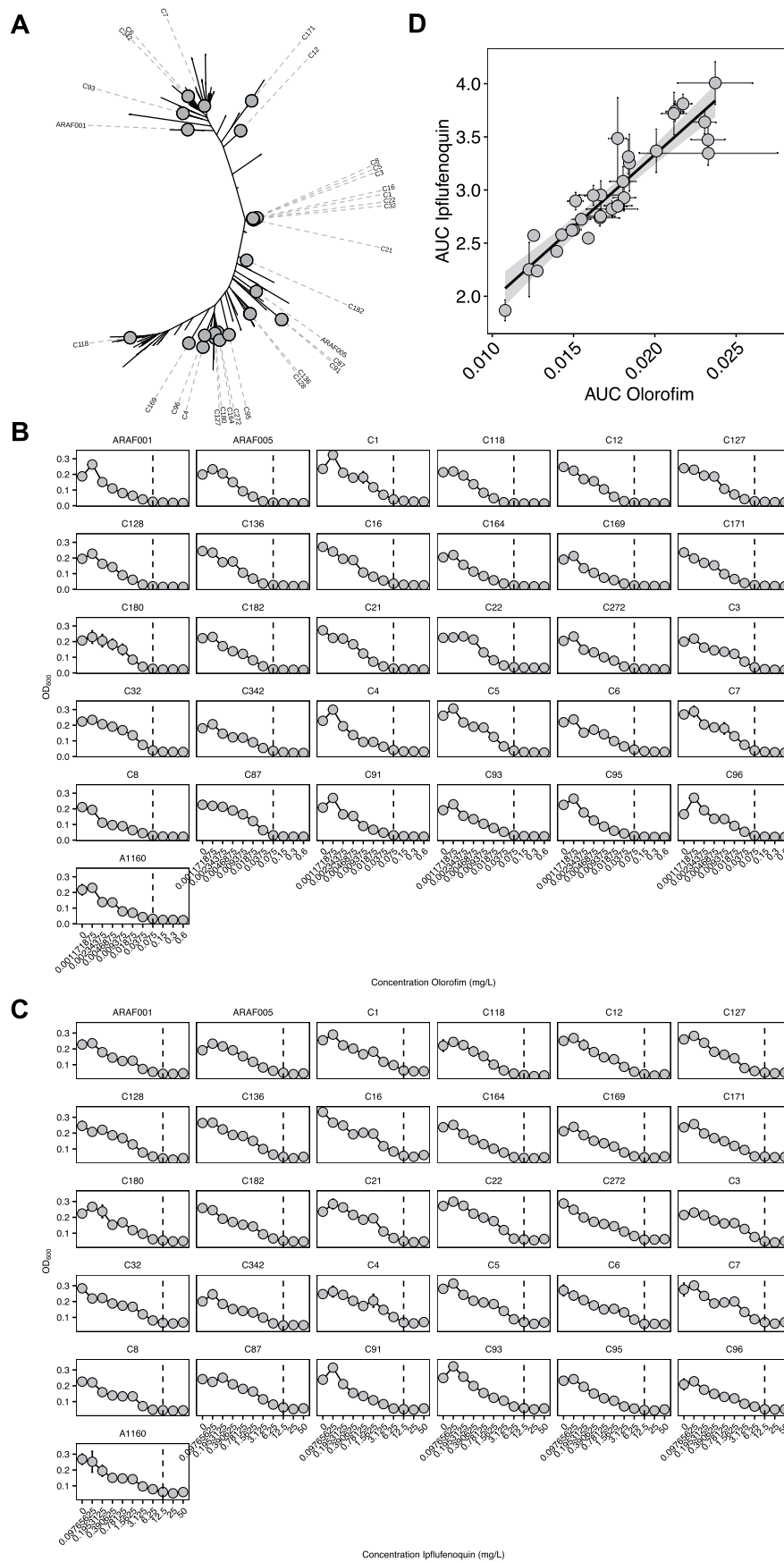
Publisher's note Springer Nature remains neutral with regard to jurisdictional claims in published maps and institutional affiliations.

Open Access This article is licensed under a Creative Commons Attribution 4.0 International License, which permits use, sharing, adaptation, distribution and reproduction in any medium or format, as long as you give appropriate credit to the original author(s) and the source, provide a link to the Creative Commons license, and indicate if changes were made. The images or other third party material in this article are included in the article's Creative Commons license, unless indicated otherwise in a credit line to the material. If material is not included in the article's Creative Commons license and your intended use is not permitted by statutory regulation or exceeds the permitted use, you will need to obtain permission directly from the copyright holder. To view a copy of this license, visit <http://creativecommons.org/licenses/by/4.0/>.

© The Author(s) 2023

	RPMI-1640		RPMI-1640 + U/U	
	Olorofim	Ipflufenoquin	Olorofim	Ipflufenoquin
MFIG001	0.06	12.5	>0.3	>50
G119C	>0.3	>50	>0.3	>50
G119S	>0.3	>50	>0.3	>50
G119A	>0.3	>50	>0.3	>50
H116R	>0.3	>50	>0.3	>50
L164P	>0.3	>50	>0.3	>50
V200E	>0.3	>50	>0.3	>50
H116R-2	>0.3	>50	>0.3	>50
L164P-2	>0.3	>50	>0.3	>50
V200E-2	>0.3	>50	>0.3	>50

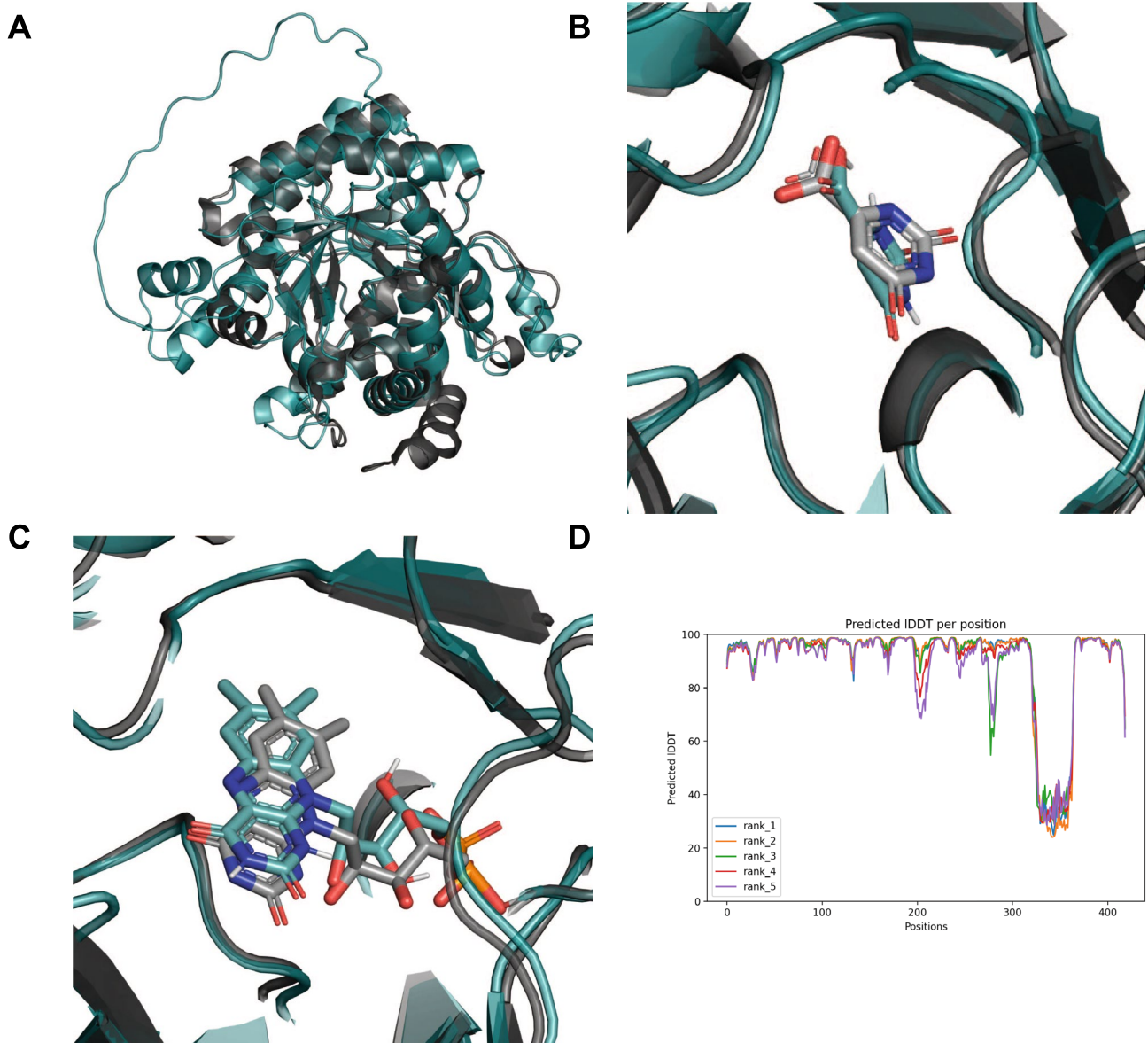
Extended Data Fig. 1 | MIC determination of olorofim and ipflufenoquin. MIC determination of olorofim and ipflufenoquin against G119 variants of *A. fumigatus*. Three biological replicates were assessed.



Extended Data Fig. 2 | See next page for caption.

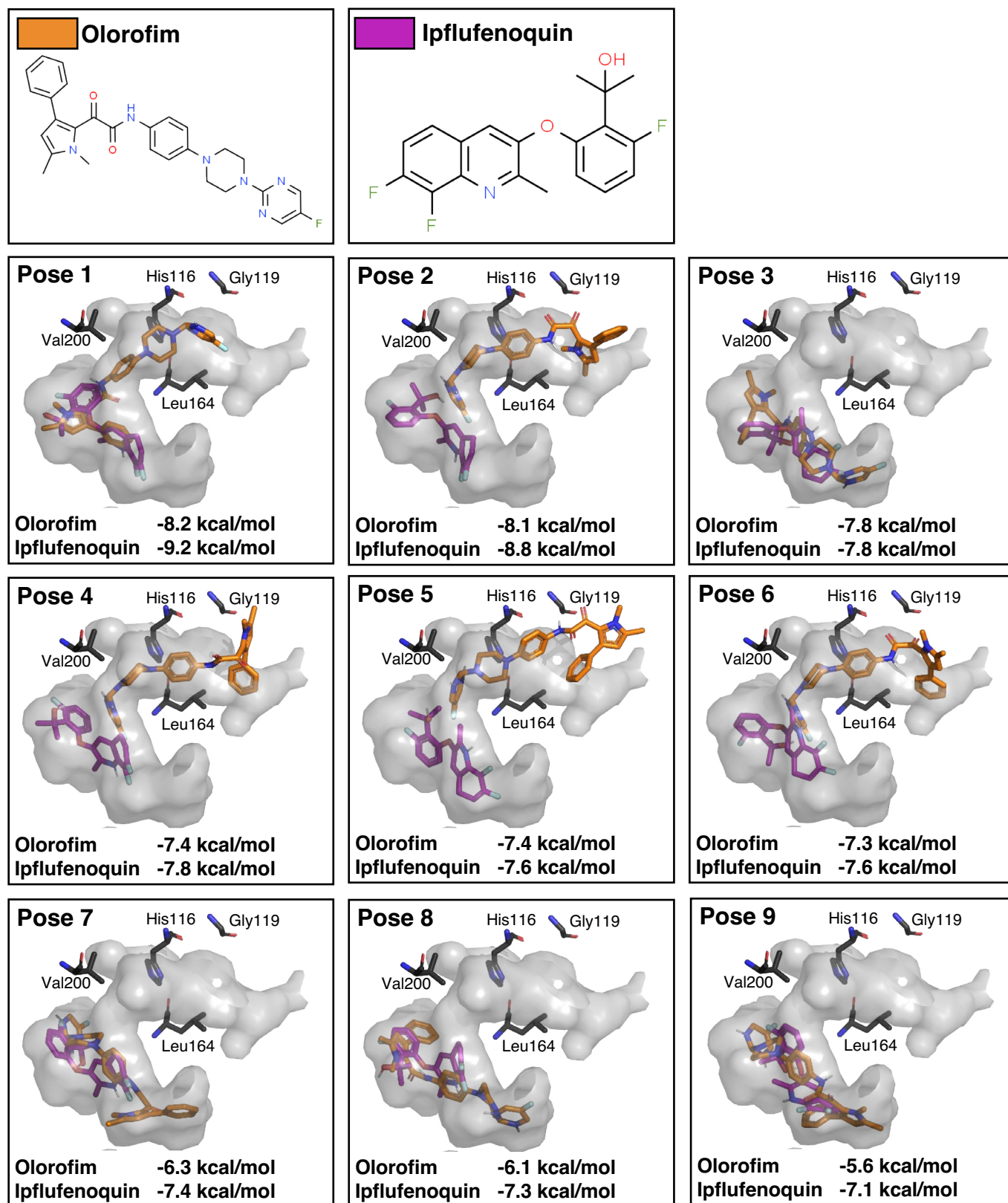
Extended Data Fig. 2 | MIC determination for natural *A. fumigatus* isolates of olorofim and ipflufenquin. A: Phylogenetic tree highlighting natural *A. fumigatus* isolates used (n = 30) sampled across a wide genetic diversity of the species, tree generated in Rhodes et al.⁵. B and C: MIC determination of olorofim (B) and ipflufenquin (C) against thirty natural *A. fumigatus* isolates.

Three biological replicates were assessed per isolate. Data are presented as the mean with SEM. The MIC is shown as a dotted line. D: Correlation of the AUC to ipflufenquin and olorofim of the 30 natural *A. fumigatus* isolates. Three biological replicates were assessed per isolate. Data are presented as the mean with SEM.



Extended Data Fig. 3 | An AlphaFold2 model of *A. fumigatus* DHODH. A: superposition of human DHODH (PDB: 2PRH_1, grey) and *A. fumigatus* DHODH (teal). The *A. fumigatus* DHODH modelled region was Asp110-Leu523, which included a region of low per-residue confidence scores (pIDDT), Arg426-Val478, which is shown as a long loop. hDHODH and *A. fumigatus* DHODH share 35% identity and 84% coverage across the full-length sequences. B: co-crystal structure of hDHODH (grey) in complex with orotate, shown in grey. The predicted pose of orotate from molecular docking with *A. fumigatus* DHODH (teal) is superimposed. C: co-crystal

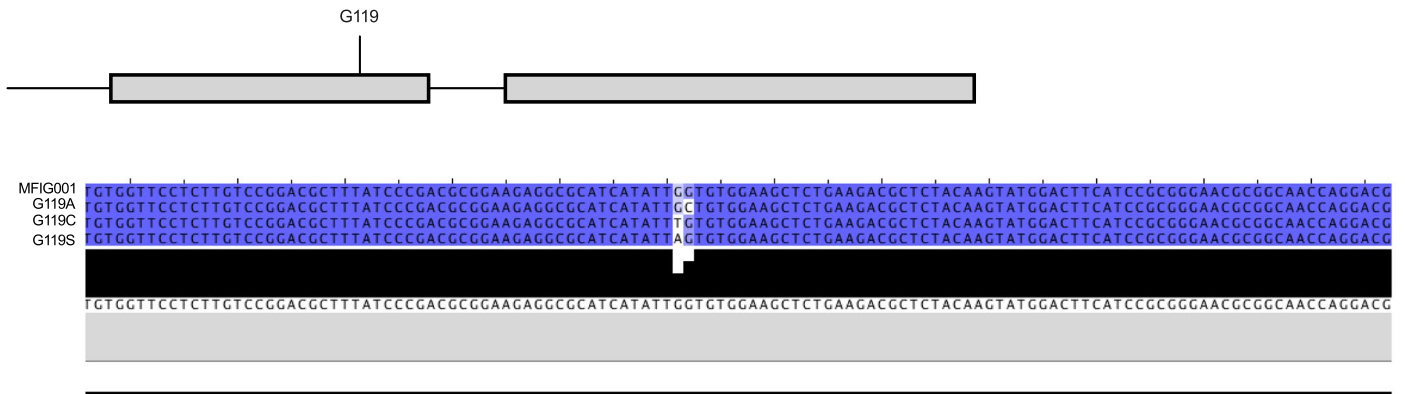
structure of hDHODH (grey) in complex with FMN, shown in grey. The predicted pose of FMN from molecular docking with *A. fumigatus* DHODH (teal) is superimposed. D: Predicted pIDDT for 5 predicted structures from AlphaFold2. We used the rank 1 model. A score of <50 is considered very low confidence. Models show a region of low per-residue confidence, Arg316-Val368, which is shown as a long loop (A). However, this region was distal to the binding pocket discussed and therefore not of functional relevance to this work.



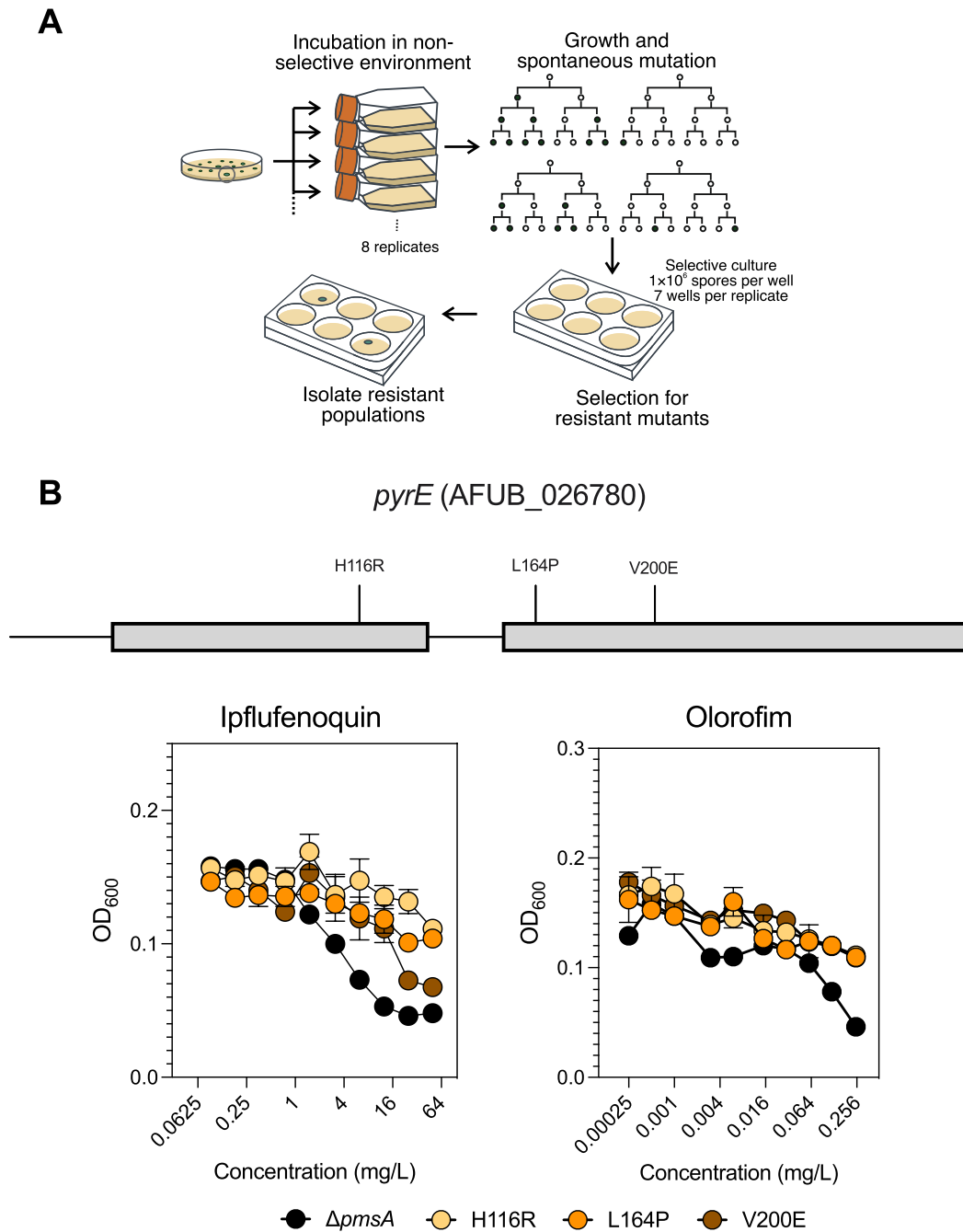
Extended Data Fig. 4 | Rank 9 AfDHODH docking models. Olorofim and ipflufenoquin were docked to the predicted active site of AfDHODH using VSPipe with the standard parameters. The top 9 poses are shown with orlorofim in

magenta and ipflufenoquin in orange. Binding energies and residues relevant for decreased susceptibility to orlorofim and ipflufenoquin are displayed for each pose.

pyrE (AFUB_026780)

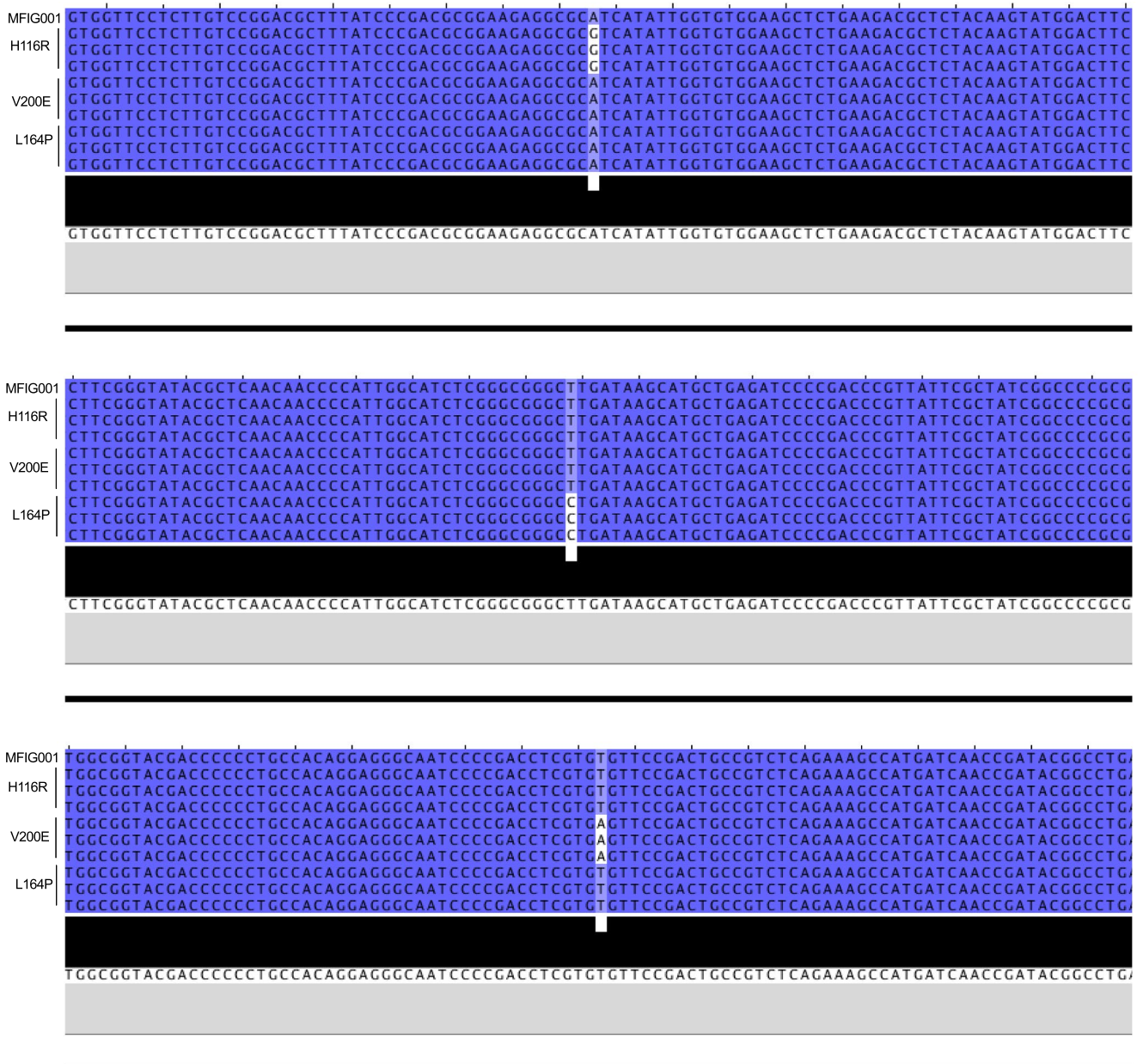


Extended Data Fig. 5 | Sanger sequencing validation of G119 variants. The *pyrE* gene was amplified by PCR and Sanger sequencing over the G119 position was performed. No other mutations within the *pyrE* coding region were observed.

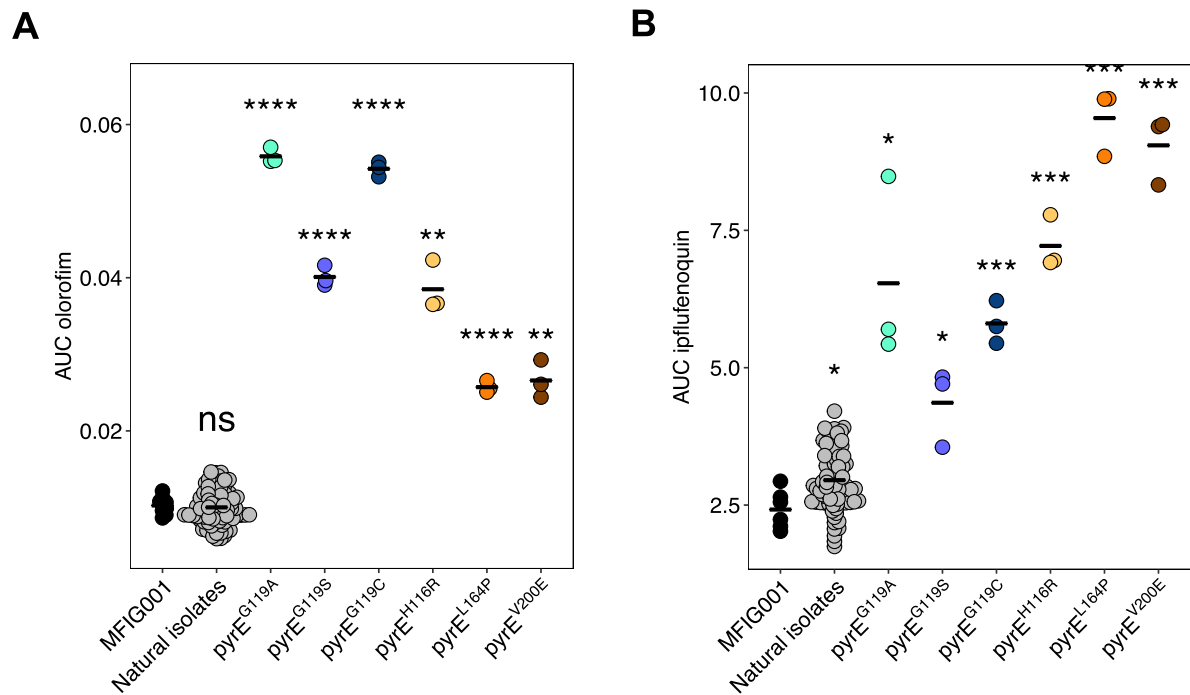


Extended Data Fig. 6 | Determination of ipflufenquin and orlorofim against *pmsA* mutants. A) workflow of fluctuation assays in *A. fumigatus*. Non-selective environment generate a genetically diverse population, for which resistant mutants are selected for on ipflufenquin containing medium.

B) MIC determination of orlorofim and ipflufenquin against G119 variants of *A. fumigatus* according to EUCAST methodology. OD₆₀₀ was measured after 48 hours. Three biological replicates were assessed. Data are presented as the mean with SEM.

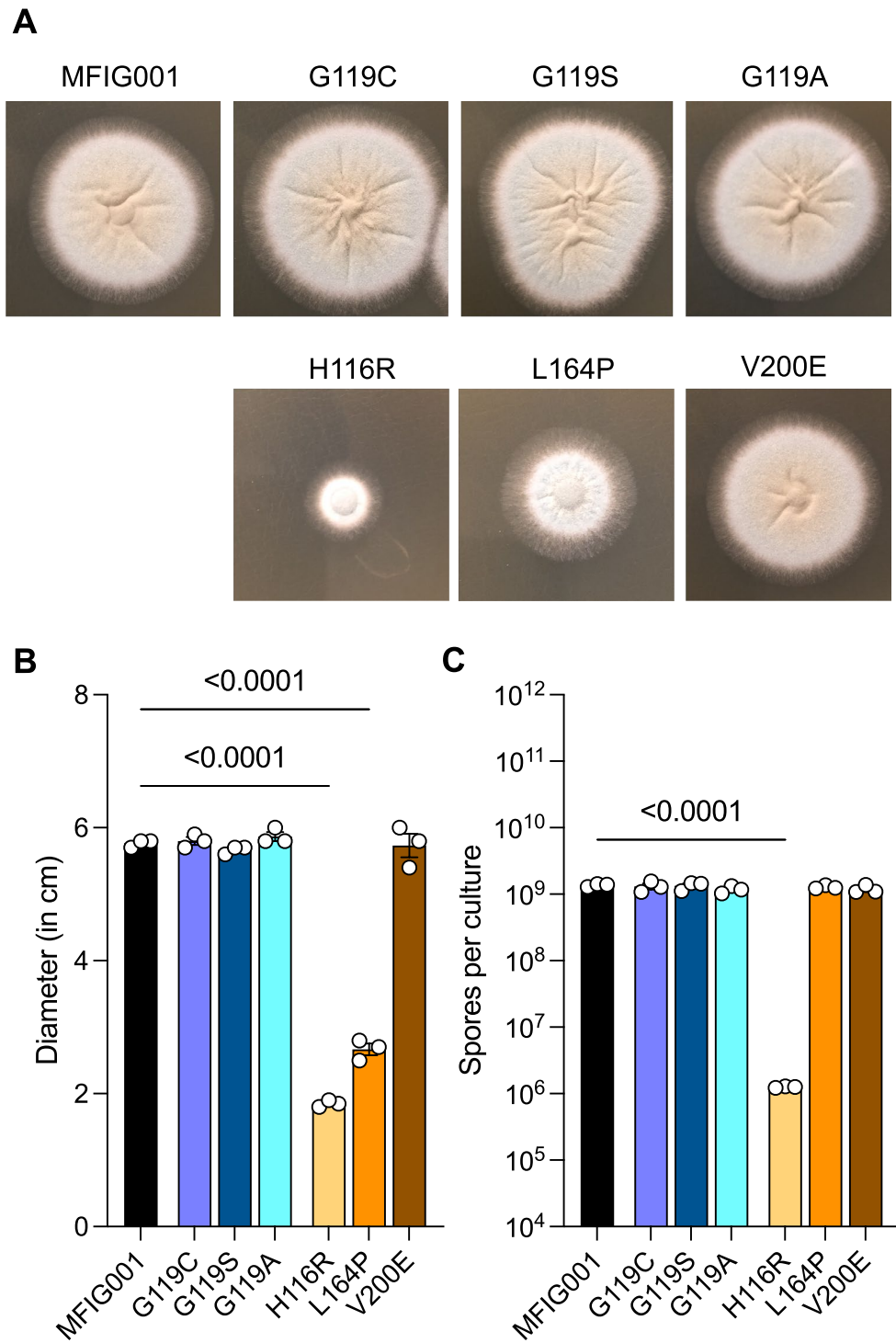


Extended Data Fig. 7 | Sanger sequencing validation of H116R, L164P and V200E variants. The *pyrE* gene was amplified by PCR and Sanger sequencing over the H116, L164 and V200 position was performed. No other mutations within the *pyrE* coding region were observed.



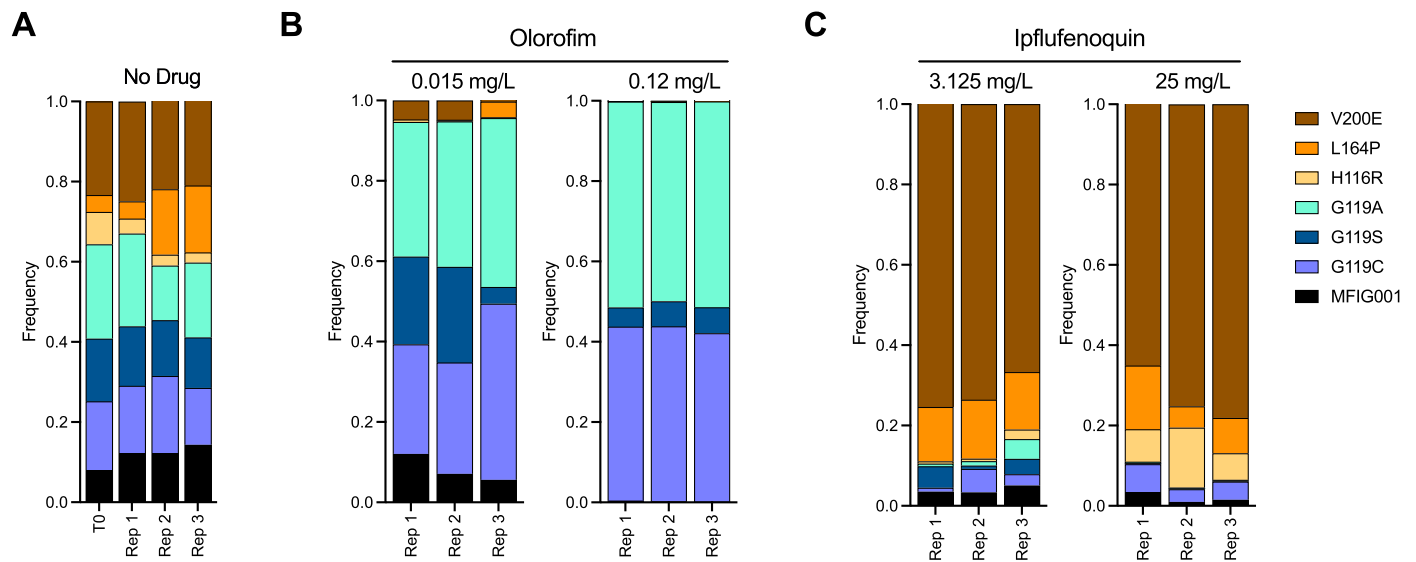
Extended Data Fig. 8 | AUC analysis of *A. fumigatus* isolates to olorofim and ipflufenquin. AUC of MIC curves to A: olorofim and B: ipflufenquin presented in Figs. 1, 2 and Extended Data Fig. 2. Each point represents an independent replicate (N = 3 for *pyrE* mutants, N = 90 for natural isolates, N = 6 for MFIG001). Crossbar shows the mean within groups. Significant differences between

groups calculated using two-sided *t*-tests with Bonferroni correction for multiple comparisons, * < 0.05, ** < 0.01, *** < 0.001, (ANOVA A: olorofim $F_{7,109} = 511$, $p < 0.0001$, B: ipflufenquin $F_{7,109} = 141$, $p < 0.0001$ (pairwise comparisons in Source Data)).



Extended Data Fig. 9 | Phenotypic characterisation of resistant mutants. A) Representative images of spot assays on Sabouraud agar medium of MFIG001 and mutant isolates. B) Radial growth was measured after 48 hours on Sabouraud agar medium. Data are presented as the mean \pm s.d. of three experiments. *P* values were determined by two-sided ANOVA with Tukey multiple comparison

between means from a sample size of $n = 3$. C) Sporulation was measured after 3 days by inoculating MM cultures with equal spores. Spores were harvested through Miracloth and counted on a haemocytometer. Data are presented as the mean \pm s.d. of three experiments. *P* values were determined by two-sided ANOVA from a sample size of $n = 3$.



Extended Data Fig. 10 | Competitive fitness in liquid RPMI-1640. A) Relative abundance of MFIG001 and mutants in RPMI-1640. Abundance was calculated as the amount of reads per isolate normalised to total QC-passed sequencing reads. Data are presented for independent replicates of three experiments. B) Abundance of MFIG001 and mutants in low (0.015 mg/L) and high (0.12 mg/L)

olorofim challenge in a mixed inoculum competition assay. Data are presented for independent replicates of three experiments. C) Abundance of MFIG001 and mutants in low (3.125 mg/L) and high (25 mg/L) ipflufenquin challenge in a mixed inoculum competition assay. Data are presented for independent replicates of three experiments.

Reporting Summary

Nature Portfolio wishes to improve the reproducibility of the work that we publish. This form provides structure for consistency and transparency in reporting. For further information on Nature Portfolio policies, see our [Editorial Policies](#) and the [Editorial Policy Checklist](#).

Statistics

For all statistical analyses, confirm that the following items are present in the figure legend, table legend, main text, or Methods section.

- | n/a | Confirmed |
|-------------------------------------|--|
| <input type="checkbox"/> | <input checked="" type="checkbox"/> The exact sample size (n) for each experimental group/condition, given as a discrete number and unit of measurement |
| <input type="checkbox"/> | <input checked="" type="checkbox"/> A statement on whether measurements were taken from distinct samples or whether the same sample was measured repeatedly |
| <input type="checkbox"/> | <input checked="" type="checkbox"/> The statistical test(s) used AND whether they are one- or two-sided
<i>Only common tests should be described solely by name; describe more complex techniques in the Methods section.</i> |
| <input checked="" type="checkbox"/> | <input type="checkbox"/> A description of all covariates tested |
| <input type="checkbox"/> | <input checked="" type="checkbox"/> A description of any assumptions or corrections, such as tests of normality and adjustment for multiple comparisons |
| <input type="checkbox"/> | <input checked="" type="checkbox"/> A full description of the statistical parameters including central tendency (e.g. means) or other basic estimates (e.g. regression coefficient) AND variation (e.g. standard deviation) or associated estimates of uncertainty (e.g. confidence intervals) |
| <input type="checkbox"/> | <input checked="" type="checkbox"/> For null hypothesis testing, the test statistic (e.g. F , t , r) with confidence intervals, effect sizes, degrees of freedom and P value noted
<i>Give P values as exact values whenever suitable.</i> |
| <input checked="" type="checkbox"/> | <input type="checkbox"/> For Bayesian analysis, information on the choice of priors and Markov chain Monte Carlo settings |
| <input checked="" type="checkbox"/> | <input type="checkbox"/> For hierarchical and complex designs, identification of the appropriate level for tests and full reporting of outcomes |
| <input checked="" type="checkbox"/> | <input type="checkbox"/> Estimates of effect sizes (e.g. Cohen's d , Pearson's r), indicating how they were calculated |

Our web collection on [statistics for biologists](#) contains articles on many of the points above.

Software and code

Policy information about [availability of computer code](#)

Data collection The sequencing data were generated via the Illumina iSeq sequencing platform.

Data analysis The sequencing data were trimmed using Trimmomatic version 0.38.0 and aligned to reference using HISAT2 version 2.2.1. Frequency of SNPs were analysed using IGV version 2.8.13. Statistical analysis was performed using Graphpad PRISM version 9. IC50 curves were analysed using XLfit 5.5.0 (IDBS). The structure of DHODH was determined using AlphaFold 2 and docking was performed using VSpice, which uses MGLTools v1.5.6 and AutoDock Vina v1.1.2. Protein structures were interpreted using PyMOL 2.5

For manuscripts utilizing custom algorithms or software that are central to the research but not yet described in published literature, software must be made available to editors and reviewers. We strongly encourage code deposition in a community repository (e.g. GitHub). See the Nature Portfolio [guidelines for submitting code & software](#) for further information.

Data

Policy information about [availability of data](#)

All manuscripts must include a [data availability statement](#). This statement should provide the following information, where applicable:

- Accession codes, unique identifiers, or web links for publicly available datasets
- A description of any restrictions on data availability
- For clinical datasets or third party data, please ensure that the statement adheres to our [policy](#)

All source data is provided via supplementary files or a Source Data file for all Figures. Raw sequencing reads are available via SRA: PRJNA961782. Human DHODH PDB file was used from: 2PRH_1 (<https://www.rcsb.org/structure/2prh>)

Human research participants

Policy information about [studies involving human research participants and Sex and Gender in Research](#).

Reporting on sex and gender

NA

Population characteristics

NA

Recruitment

NA

Ethics oversight

NA

Note that full information on the approval of the study protocol must also be provided in the manuscript.

Field-specific reporting

Please select the one below that is the best fit for your research. If you are not sure, read the appropriate sections before making your selection.

- Life sciences Behavioural & social sciences Ecological, evolutionary & environmental sciences

For a reference copy of the document with all sections, see [nature.com/documents/nr-reporting-summary-flat.pdf](https://www.nature.com/documents/nr-reporting-summary-flat.pdf)

Life sciences study design

All studies must disclose on these points even when the disclosure is negative.

Sample size

No sample size calculations was required for this study but our sample sizes are similar to (or larger than) those reported in previous publications. Representative publications are mentioned below:

<https://doi.org/10.1073/pnas.1608304113>

<https://doi.org/10.1038/s41467-019-14191-1>

Data exclusions

No data were excluded from this study.

Replication

All experiments were conducted with independent biological replicates. The number of independent replicates were consistent with similar experiments conducted within the field. All experiments had a minimum of three independent biological replicates. Fluctuation tests were replicated 8 times in order to achieve 9 independent ipflulenequin resistant mutants. N values are reported in figure legends, and all plots show variation as SEM error bars

Randomization

No randomization was applied as this was impossible for the in vitro experimentation. Covariates were controlled by including relevant controls in experiments.

Blinding

Blinding and group allocations were not required or performed in this study. Data collection and analysis was performed by the same person who was not blinded to the conditions of the experiments. Biological experiments were impossible to conduct under the conditions of blinding. Hence, there was no blinding.

Reporting for specific materials, systems and methods

We require information from authors about some types of materials, experimental systems and methods used in many studies. Here, indicate whether each material, system or method listed is relevant to your study. If you are not sure if a list item applies to your research, read the appropriate section before selecting a response.

Materials & experimental systems

- | n/a | Included in the study |
|-------------------------------------|--|
| <input checked="" type="checkbox"/> | <input type="checkbox"/> Antibodies |
| <input checked="" type="checkbox"/> | <input type="checkbox"/> Eukaryotic cell lines |
| <input checked="" type="checkbox"/> | <input type="checkbox"/> Palaeontology and archaeology |
| <input checked="" type="checkbox"/> | <input type="checkbox"/> Animals and other organisms |
| <input checked="" type="checkbox"/> | <input type="checkbox"/> Clinical data |
| <input checked="" type="checkbox"/> | <input type="checkbox"/> Dual use research of concern |

Methods

- | n/a | Included in the study |
|-------------------------------------|---|
| <input checked="" type="checkbox"/> | <input type="checkbox"/> ChIP-seq |
| <input checked="" type="checkbox"/> | <input type="checkbox"/> Flow cytometry |
| <input checked="" type="checkbox"/> | <input type="checkbox"/> MRI-based neuroimaging |